Viscoelastic and Biomechanical Properties of Osteochondral Tissue Constructs Generated From Graded Polycaprolactone and Beta-Tricalcium Phosphate Composites

Cevat Erisken[1]
e-mail: ce2213@columbia.edu

Dilhan M. Kalyon[2]
e-mail: dkalyon@stevens.edu

Hongjun Wang
e-mail: hongjun.wang@stevens.edu

Stevens Institute of Technology,
Hoboken, NJ 07030

The complex micro-/nanostructure of native cartilage-to-bone insertion exhibits gradations in extracellular matrix components, leading to variations in the viscoelastic and biomechanical properties along its thickness to allow for smooth transition of loads under physiological movements. Engineering a realistic tissue for osteochondral interface would, therefore, depend on the ability to develop scaffolds with properly graded physical and chemical properties to facilitate the mimicry of the complex elegance of native tissue. In this study, polycaprolactone nanofiber scaffolds with spatially controlled concentrations of β-tricalcium phosphate nanoparticles were fabricated using twin-screw extrusion-electrospinning process and seeded with MC3T3-E1 cells to form osteochondral tissue constructs. The objective of the study was to evaluate the linear viscoelastic and compressive properties of the native bovine osteochondral tissue and the tissue constructs formed in terms of their small-amplitude oscillatory shear, unconfined compression, and stress relaxation behavior. The native tissue, engineered tissue constructs, and unseeded scaffolds exhibited linear viscoelastic behavior for strain amplitudes less than 0.1%. Both native tissue and engineered tissue constructs demonstrated qualitatively similar gel-like behavior as determined using linear viscoelastic material functions. The normal stresses in compression determined at 10% strain for the unseeded scaffold, the tissue constructs cultured for four weeks, and the native tissue were 0.87 ± 0.08 kPa, 3.59 ± 0.34 kPa, and 210.80 ± 8.93 kPa, respectively. Viscoelastic and biomechanical properties of the engineered tissue constructs were observed to increase with culture time reflecting the development of a tissuelike structure. These experimental findings suggest that viscoelastic material functions of the tissue constructs can provide valuable inputs for the stages of in vitro tissue development.
[DOI: 10.1115/1.4001884]

Keywords: functionally graded, interface, osteochondral, scaffold, tissue engineering, electrospinning

1 Introduction

Articular cartilage injuries are quite common conditions affecting millions of people and are complicated further by the inability of adult articular cartilage to regenerate [1]. Without any treatment, articular cartilage does not heal or heals to form a tissue with inferior mechanical properties that may eventually lead to osteoarthritis. Although primary joint arthroplasty has shown a reasonable degree of success to date, relatively high failure rates after 10 years post implantation have also been reported [2–5] mainly due to wear [6,7] and bacterial infections [8] of nonbiodegradable materials. In this sense, biological repair of the joints using tissue engineering methods would present suitable alternatives [9,10]. In tissue engineering, the repair or regeneration of the osteochondral defects involves regenerating the cartilage and bone tissue concomitantly by growing appropriate cells on properly designed biodegradable scaffolds which can be possibly incorporated with a variety of growth factors or promoters. However, major challenges currently remain in the engineering of scaffolds due to the difficulties in generating the natural gradations in porosity, composition, and biomechanical and viscoelastic properties associated with native tissue. In the area of osteochondral tissue repair, success will, therefore, depend on the ability to meet the grading requirements of two different tissues, i.e., cartilage and bone, as well as the interface between the two [11].

The cartilage-bone interface is a highly complicated structure due to the physical, chemical, as well as biological variations observed as a function of distance from the articulating surface to the subchondral bone. Regarding physical properties, for example, the orientation of the collagen fibers, calcium phosphate mineral particles and cells are different at various distances from the articular surface. The collagen fibrils run in vertical directions to the interface in the calcified cartilage region while they are parallel to it in the regions close to the surface [12,13]. Similarly, the chondrocytes are organized in parallel to the interface at the surface

[1]Present address: Department of Biomedical Engineering, Columbia University, New York, NY 10027

[2]Corresponding author.

Contributed by the Bioengineering Division of ASME for publication in the JOURNAL OF BIOMECHANICAL ENGINEERING. Manuscript received September 14, 2009; final manuscript received April 29, 2010; accepted manuscript posted May 27, 2010; published online September 1, 2010. Assoc. Editor: Stephen Klisch.

and vertical to it at the calcified region [13]. The calcium particles, on the other hand, are aligned perpendicular to the interface in cartilage and parallel to it in the bone [14]. As for the chemical composition of collagen fibers, mineral particles, and cells at the cartilage-bone interface, similar variations were also reported. The collagen fibrils were determined to be denser at the articular surface [12], while the concentration of calcium particles tends to increase toward the bone tissue [15]. As far as the biological properties are concerned, the cartilage-bone interface contains cells having a chondrogenic phenotype on the cartilage side, osteoblastic phenotype on the bone side, and multiple phenotypes in a spatially organized fashion in between [16].

The biomechanical properties of the native osteochondral tissue have been extensively studied using compressive [17–20], tensile [21,22], and shearing [23,24] deformations together with depth-dependent variations in the biomechanical properties [25,26]. For example, Oloyede and Broom [19] determined that the time-dependent response of the native tissue to an applied load depends on the time dependence of the exudation of the water and effective consolidation of the collagen fibrillar meshwork and the proteoglycans. These studies are important in terms of defining the biomechanical behavior of the joints in response to cyclic tensile, compressive, and shearing deformations during walking and other daily activities [27]. Similarly, the viscoelastic behavior of the native cartilage-bone tissue has also been studied both experimentally and theoretically under tensile and compressive [28–33], as well as torsional [23,24,34] types of shearing.

Recent investigations have also focused on the ability to engineer the cartilage-bone interface in an attempt to mimic the characteristics of the native tissue. Schaefer et al. [35], for example, prepared two individual sheets consisting of polyglycolic acid on one side and a blend of poly-lactic-co-glycolic acid (PLGA) and polyethylene glycol (PEG) on the other, and then seeded the two sides with chondrocytes and periosteal cells, respectively. They then sutured the two constructs together to obtain three-dimensional cartilage/bone composites after 1 week of culture period. No characterization of the viscoelastic and biomechanical properties of these constructs were reported.

In another study, Gao et al. [36] prepared sheets of spongy hyaluronan and porous calcium phosphate, joined them using a fibrin sealant, and then implanted them into a subcutaneous pocket in syngeneic rats. They harvested the implants at 3 and 6 weeks after insertion in order to examine their morphological features and for types I, II, and X collagen, but the biomechanical properties of the constructs were not taken into consideration. Later, Sherwood et al. [37] designed and manufactured cartilage/bone scaffolds by layering three different materials composed of D,L-PLGA/L-PLA for cartilage, L-PLGA/TCP for bone, and a blend of these materials for the bone-cartilage transition zone. They reported that the tensile strength of the L-PLGA/TCP side of the scaffold was similar to fresh cancellous human bone. There was no mechanical testing of the tissue constructs obtained upon the seeding of the scaffolds with chondrocytes.

More recently, Hung et al. [38] developed native-joint shaped tissue constructs from bilayered scaffolds of chondrocyte-seeded agarose on natural trabecular bone, and tested the constructs under confined and unconfined compressions. With increasing culturing time, the constructs exhibited increased Young's modulus (in unconfined compression) and aggregate modulus (in confined compression) values. In another study by Klein et al. tissue was engineered using commercially available 6.5 mm polycarbonate membrane inserts with uniform pore size of 0.4 μm as scaffolds. They harvested cells from articular cartilage and seeded them onto the inserts either by layering or mixing. Confined compression testing of the engineered tissue constructs yielded soft regions at both ends of the constructs in contrast to the native tissue, which exhibited increasing compressive moduli with depth. Furthermore, the formation of tissue constructs has also been investigated under load, and it was suggested that the presence of such loads enhances relevant extracellular matrix formation due to similarities between the environment generated during tissue construct formation and the physiology of the native tissue [20,39,40].

Taken together, the common denominator in most of these earlier studies was the engineering of cartilage tissues onto a more rigid substrate, which served as a mechanically stable bone-interfacing component. In such an approach, the osteochondral interface is considered to consist of two separate phases, where soft component represents cartilage while hard component represents the bone. In addition, the resulting engineered tissue constructs were not subjected to detailed biomechanical characterization presumably because measuring the material properties of the cell-seeded constructs integrated with the rigid component backing would not have provided reliable results that are representative of the engineered tissue. Here, we have utilized the capabilities of a recently developed extrusion-electrospinning technique [41] to generate mineral concentration gradations within the confines of unitary scaffolds to better mimic the structure of native osteochondral interface.

It is anticipated that the viscoelastic properties of the tissues engineered in this study could provide a better understanding of the development of extracellular matrix since the scaffolds employed here are designed to give rise to the hard component in a graded manner. The temporal variations in the viscoelastic properties (obtained in conjunction with unconfined compression, small-amplitude oscillatory shear, and stress relaxation upon step compression) of the engineered tissue constructs were characterized and compared with those of native bovine osteochondral tissue. The characterization of the viscoelastic properties of the cell-seeded scaffolds with time should provide insight into the development stages of the tissue-like structures and their potential implementation for the regeneration/repair of damages associated with osteochondral interfaces.

2 Materials and Methods

2.1 Scaffold Preparation and Characterization. Scaffolds were fabricated employing a hybrid twin-screw extrusion/electrospinning (TSEE) process, which we have developed and consists of a twin-screw extruder with fully intermeshing and corotating screws (Material Processing & Research, Inc., Hackensack, NJ) integrated with the electrospinning process [42]. The apparatus is suitable for the generation of functionally graded scaffolds since the time-dependent feeding of the ingredients can give rise to differences in the composition, porosity, and mechanical properties. Here the polycaprolactone was first dissolved in dichloromethane (DCM) at a ratio of 12/100 (g/ml). The PCL/DCM solution was then fed through one of the injection points available on the barrel of the extruder into the first mixing zone in which β-TCP nanoparticles were also introduced from another injection point. The ability to control the feed rates of the PCL/DCM solution and β-TCP nanoparticles in a time-dependent fashion enabled the generation of continuously varying β-TCP concentrations in the nonwoven mesh. The nonwoven meshes were punched into circular disks of 8 mm in diameter to serve as scaffolds for the tissue constructs.

The diameter, morphology, and surface properties of the electrospun composite fibers were determined using a LEO Gemini 982 scanning electron microscope (SEM). The concentration of β-TCP incorporated into the electrospun PCL-β-TCP scaffolds was measured using a thermogravimetric analysis apparatus (TGA-Q50, TA Instruments of New Castle, Delaware) upon complete degradation of PCL by heating from 25°C to 550°C at 15°C/min under N_2 atmosphere. Energy dispersion X-ray (EDX) and energy dispersive spectroscopy (EDS) of the scaffolds were also conducted under SEM upon scanning for 150 s duration at 10 kV to validate the presence of β-TCP nanoparticles.

2.2 Cell Culture and Tissue Formation. The scaffolds were sterilized by immersing into graded concentrations of ethanol (70–

100%) with 10% increments and then washed with phosphate-buffered saline (PBS) solution. The MC3T3-E1 mouse preosteoblast cells (ATCC, Manassas, VA) were seeded onto the scaffolds placed in a 24-well plate at a density of 20,000 cells/cm^2 ($\sim$47,500 cells/scaffold). A total of 1 ml of complete medium containing MEM Alpha Medium (Invitrogen, Carlsbad, CA), which was further supplemented with fetal bovine serum (Gibco-Invitrogen, Carlsbad, CA) and penicillin/streptomycin (1/0.1/0.01 volume ratio, respectively) was added to immerse the scaffolds completely. The cell-scaffold constructs were then incubated at 37°C and 5% CO_2. The medium was replaced with osteogenic differentiation medium, MEM Alpha Medium, which was further supplemented with fetal bovine serum, penicillin/streptomycin (1/0.1/0.01 volume ratio, respectively) and $NaHCO_3$ (2.2 g/l) after culturing in complete medium for three days. The engineered tissue constructs were harvested after culture periods of 1 and 4 weeks, preserved in 4% buffered formaldehyde solution until use in SEM and for biomechanical and viscoelastic characterization. Additional information on the preparation of the tissue constructs can be found elsewhere [41].

2.3 Native Cartilage-Bone Specimen Preparation. Fresh bovine knee joints were obtained from a local abattoir and stored at −80°C until the day of characterization. Joints were removed and thawed at room temperature for approximately 12 h before preparation of specimens. The articular surfaces were drilled by using a slowly-rotating drill press to which a cork borer with an inner diameter of 8 mm was integrated, to a depth ($\sim$3 mm) such that cartilage-bone interface could be harvested from the surface. The subchondral regions of these specimens were then removed. Samples gathered by this method were equilibrated in PBS solution at 4°C until the time of characterization. Eight samples were removed from the patellar surface of each femur. Before the test, the thickness of each sample was measured with an electronic micrometer at four different locations, and samples with 100 μm or more variations were discarded. All measurements were carried out at 37°C.

2.4 Characterization of Viscoelastic Material Functions Under Shear and Compression. The samples were characterized in compression and shear using an advanced rheometric expansion system (ARES) Rheometer (TA Instruments). During the experiments the specimen was sandwiched between two rheometer disks (8 mm diameter), one of which either oscillates (consecutive clockwise and counterclockwise cycles) or translates in the downward direction at constant velocity while the second disk remains stationary (Fig. 1). The specimen was immersed in PBS solution kept at 37°C. This arrangement was used to prevent drying of the specimens [34] of the native tissue and the tissue constructs during the compression and shearing experiments. The PBS containing chamber consisted of two concentric cylindrical dishes, one of which was sealed and attached to the lower fixture (which is connected to the torque and normal force transducer) and the second was attached to the upper fixture of the rheometer, which was coupled to the motor (Fig. 1).

2.4.1 Biomechanical Characterization Upon Compression. Unconfined uniaxial compression of the native tissues, engineered tissue constructs, and unseeded PCL-β-TCP scaffolds was performed in the compressive nominal strain range of 0–10% at a constant compression rate of 0.05 mm/min. This strain level was previously used in biomechanical characterizations of native and engineered tissues [43–45]. During the compression experiments the specimens were first squeezed to a normal force of approximately 0.03 N to assure full contact, after which the compression test was initiated. In a second set of experiments the relaxation behavior of native tissue and tissue constructs were characterized upon compression using a nominal step strain that is applied in 2–3.5 s.

2.4.2 Small-Amplitude Oscillatory Shear. During oscillatory shearing of a stable specimen between two disks, one of which is oscillating and the second stationary, the dynamic properties are obtained independent of time. However, if the specimen is not stable for any reason, i.e., cross-linking, loss of water, oxidation etc., a time scan whereby the frequency and the strain amplitude are held constant reveals changes in the dynamic properties with time, since the dynamic properties are very sensitive to changes in the structure. Dynamic time-sweep experiments were carried out to ensure the stability of the specimens held in PBS during the dynamic shear tests. In these experiments the linear viscoelastic material functions were analyzed for a period of 1000 s. In small-amplitude oscillatory shear experiments, a dynamic strain-sweep between strain amplitudes of 0.1% and 100% was performed at a frequency of 1 rps to determine the limit of linear viscoelastic range.

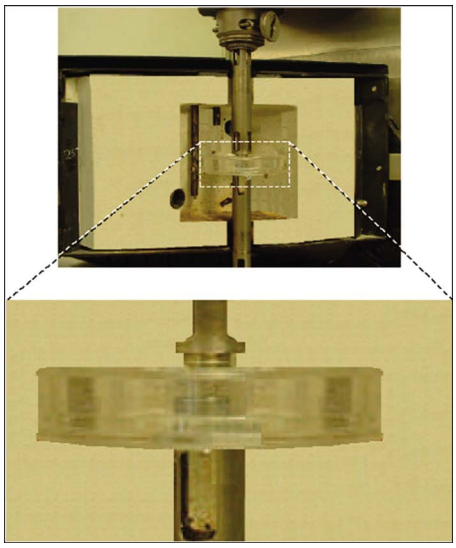

Fig. 1 Experimental setup for the viscoelastic and biomechanical characterization of the samples. An environmental chamber held fixtures and specimen immersed in PBS at 37°C.

In oscillatory shear, the shear strain is defined as $\gamma = \gamma_0 \sin(\omega t)$, where γ_0 is shear strain amplitude (i.e., $\theta D/h$, where θ is the angular displacement, D is the disk diameter and h is the gap in between the two disks), ω is the oscillation frequency, and t is the time. The shear stress τ response to the imposed oscillatory deformation consists of two contributions associated with the energy stored as elastic energy and energy dissipated as heat, i.e., $\tau = G'(\omega)\gamma_0 \sin(\omega t) + G''(\omega)\gamma_0 \cos(\omega t)$, where $G'(\omega)$ is the shear storage modulus and $G''(\omega)$ is the shear loss modulus. Overall, G' represents the elastic energy stored and G'' represents the energy dissipated as heat. In the region of linear viscoelasticity the values of dynamic material properties, namely, the storage modulus, the loss modulus, and the magnitude of complex viscosity, i.e., $[(G'/\omega)^2 + (G''/\omega)^2]^{1/2}$, should be independent of the strain amplitude.

Finally, the dynamic properties were characterized as a function of frequency in the range of 0.1–100 rps. The use of multiple frequencies allows the characterization of the linear viscoelastic response of the tissue over a range of time scales to provide a broad fingerprint of the viscoelastic response of the tissue. In general, at relatively small characteristic times for deformation (relatively high frequencies) the elastic response is accentuated, while at longer characteristic times (relatively low frequencies) the viscous flow behavior is accentuated.

2.5 Statistical Analysis. Statistical significance for β-TCP content as a function of scaffold thickness was tested using one-way Analysis of Variance (ANOVA) with Tukey's post hoc test

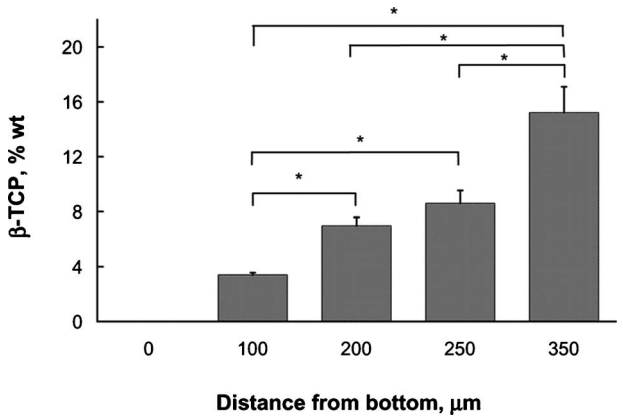

Fig. 2 Typical distribution of concentration of β-TCP nanoparticles as a function of the distance from the bottom of the scaffold (* indicates the significance between the groups at $p < 0.01$ level)

and the SPSS software package. A multivariate ANOVA test was employed for the comparison of native tissue, tissue constructs obtained at four weeks, and unseeded scaffolds in terms of the modulus and toughness (defined here as the integral of stress versus strain). The p levels at which differences between groups were considered statistically significant are defined in the captions of the relevant figures or tables.

3 Results and Discussions

3.1 Scaffold Characterization. The hybrid extrusion-electrospinning technology for the fabrication of 3D porous composite PCL-β-TCP yielded nonwoven meshes to serve as tissue engineering scaffolds. The thicknesses of the scaffolds were between 0.3 mm and 0.4 mm. The PCL fibers (200–2000 nm) constituting the scaffolds were incorporated with linearly varying concentration of β-TCP nanoparticles. Linear distribution of the concentration of the β-TCP nanoparticles as a function of depth in the scaffolds as obtained with TGA is shown in Fig. 2. The TGA results indicate that the concentration of the β-TCP changes from 0% to 15.2% by weight (6.1% by volume) between the two surfaces of the scaffold. Typical SEM micrographs of the sections of PCL-β-TCP scaffold corresponding to the bottom, middle, and top portions are shown in Figs. 3(*a*)–3(*c*), respectively.

The controlled grading of β-TCP nanoparticles into PCL nanofibers was also verified by energy dispersive spectroscopy. Figures 3(*d*)–3(*f*) show the EDX mapping associated with the bottom, center, and top sections of the typical PCL-β-TCP composite scaffold, respectively. The results of the elemental analysis are given in Figs. 3(*g*)–3(*i*) for the bottom, center, and top sections of the scaffold, respectively. The greater prevalence of the white spots in the EDX maps and the increasing areas associated with the Ca and P peaks as one moves away from the bottom surface are indicative of the increasing Ca and P concentrations associated with the increasing β-TCP nanoparticle concentrations. The increasing concentration of β-TCP from the bottom to the top surface of the scaffold is clearly indicated.

3.2 Small-Amplitude Oscillatory Shear Behavior

3.2.1 Time-Sweep Test for the Stability Analysis of the Native Tissue. The dynamic time-sweep experiments performed on the native tissue specimens for the material functions, i.e., the storage modulus (G') and the loss modulus (G''), indicated that the specimens were indeed stable at least for a period of 1000 s (Fig. 4(*a*)) during rheological characterization. It appears that the immersion of the specimens into the PBS solution was effective in preventing the drying and deterioration of the tissue samples during oscillatory shear tests. The same test performed in the absence of the PBS yielded increasing values of the storage and loss moduli with

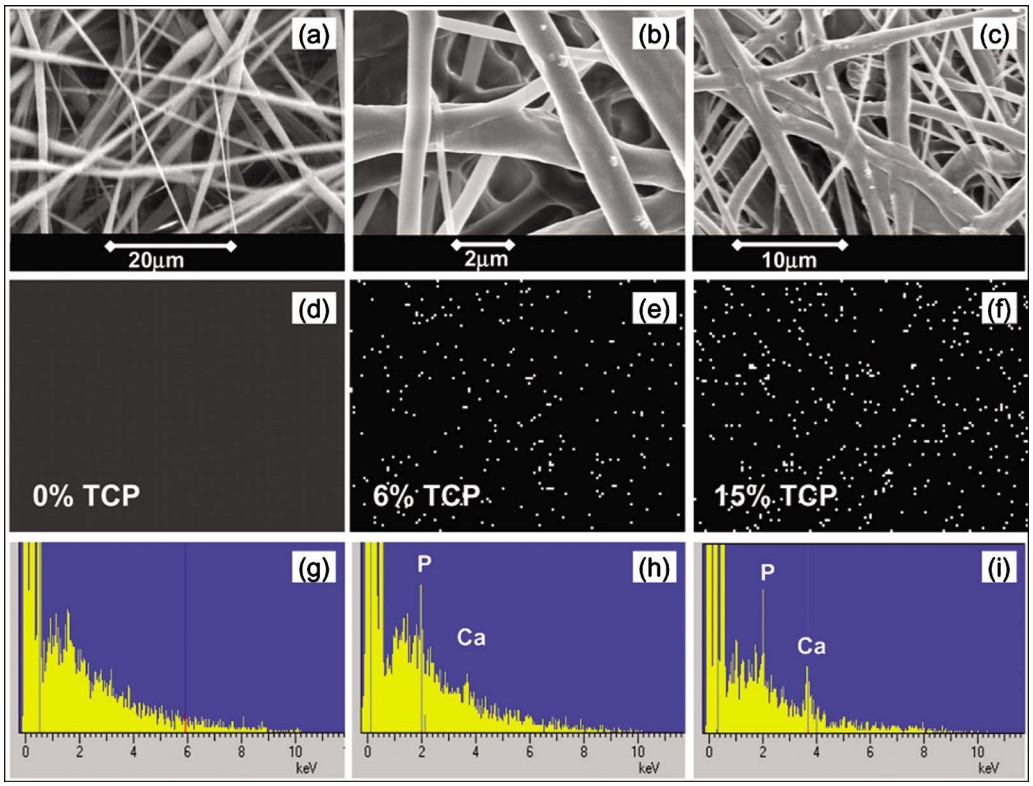

Fig. 3 SEM micrographs of the sections of PCL-β-TCP scaffold corresponding to the (*a*) bottom, (*b*) middle, and (*c*) top portions, and their respective EDX mapping ((*d*)–(*f*)) and spectrum ((*g*)–(*i*))

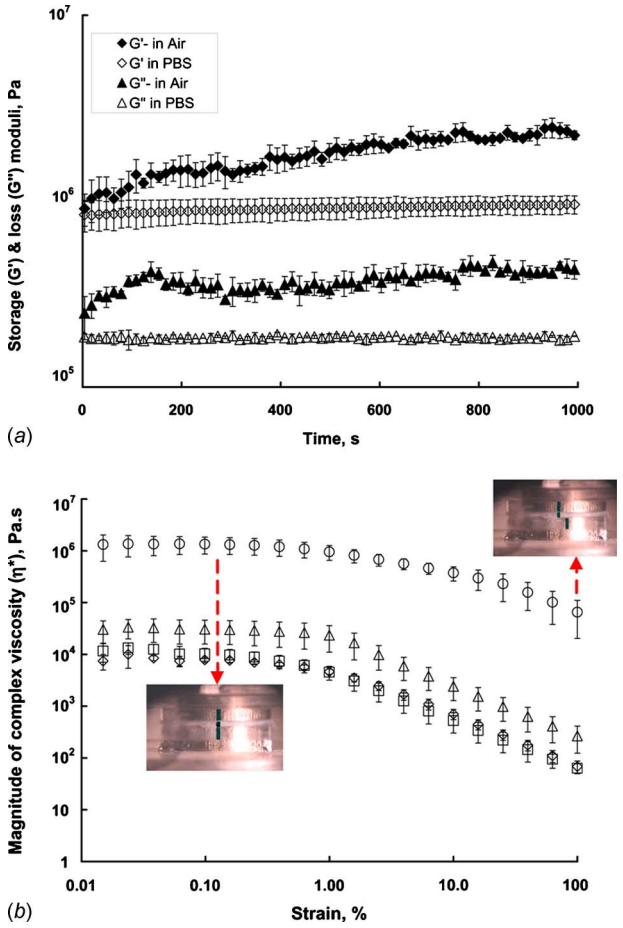

Fig. 4 (*a*) Stability analysis of the native tissue in terms of storage and loss moduli in air and in PBS solution at 1 rps, 0.1% strain, and 37°C. Error bars represent the upper and lower bounds of deviations from the mean for 95% confidence interval. (*b*) Magnitude of complex viscosity versus strain amplitude behavior of unseeded scaffolds (◇), engineered tissue constructs at one week (□) and four weeks (△), and the native bovine tissue (○), at 1 rps and 37°C. Error bars represent the upper and lower bounds of deviations from the mean for 95% confidence interval.

time suggesting drying of the specimens during oscillatory shearing in the absence of PBS immersion. The tan delta values of the native tissue during this time period were determined to be in the range of 0.19–0.22.

3.2.2 Strain-Sweep Test. The dynamic material functions, namely, the magnitude of complex viscosity, the storage modulus, and the loss modulus of the native tissue, engineered tissue constructs after 1 and 4 weeks, and those of the unseeded scaffolds were measured over the strain magnitude range of 0.01–100% at 1 rps. It was observed that the magnitude of the complex viscosity (η^*), storage modulus (G') as well as the loss modulus (G'') values remained independent of the strain amplitude up to approximately 0.1% strain. As an example, the magnitude of complex viscosity versus strain amplitude behavior of the native tissue, engineered tissue constructs, and unseeded scaffolds are shown in Fig. 4(*b*). All four experimental groups exhibited linear viscoelastic behavior for strain amplitudes less than 0.1%. However, the linear viscoelastic range was significantly smaller for the native bovine tissue versus those of the tissue constructs and unseeded scaffold samples.

The oscillatory shear behavior of the tissue constructs and native tissue were all subject to the occurrence of wall slip, which is a ubiquitous problem in the rheological characterization of biological tissues. It should be noted that the literature generally associates the dependence of the viscoelastic properties on the strain amplitude only with the linear to nonlinear transformation with increasing strain amplitude. However, as shown in Fig. 4(*b*), the native tissue and tissue constructs are prone to wall slip during oscillatory shearing. In this experiment the wall slip of the native tissue and tissue constructs during oscillatory shear were documented with a simple method involving the drawing of a straight marker line to cover the free surface of the specimen sandwiched in between the two disks as well as the edges of the two disks [46,47]. The discontinuities observed to occur at one or both surfaces with increasing strain amplitude are indicative of the occurrence of wall slip as demonstrated for the native tissue in the insets in Fig. 4(*b*).

The surface of the articular cartilage is rather soft, containing no minerals, but is highly populated with chondrocytes that secrete proteoglycan molecules to provide lubrication of the surfaces [48]. The formation of a low-viscosity lubricating layer at the wall of the rheometer gives rise to the development of an "apparent slip" mechanism, which significantly alters the distribution of the velocity and shear rate from those associated with the assumption of the no-slip condition [49]. Due to this lubricating characteristic of the biological tissues, the assumption of a no-slip condition can be very misleading as demonstrated here. This wall-slip response of the tissue constructs upon deformation could be especially important when the tissue constructs are implanted for in vivo studies. In the stage of implantation of the tissue constructs, this wall-slip effect may deter or retard the joining of the interface between the tissue construct and native tissue at the point of defect. The data reported for the linear region were free of wall-slip effects as documented with the straight-line marker method [47] and the dynamic frequency-sweep experiments were, therefore, carried out at a strain amplitude of 0.1%.

3.2.3 Relaxation Behavior. Figure 5 shows the response of the specimens of the native tissue and engineered tissue constructs cultured for 4 weeks upon 20% unconfined compression applied in 2–3.5 s. The decay in stress after imposing a nominal strain determines the time-dependent relaxation behavior of the samples. As shown in Fig. 5, the normal stress imposed on the samples decreased with time at a very small rate as compared with the rate it was initially imposed. The relaxation behavior of the native tissue was characterized by a monotonic decrease in the normal stress with time up to about 1000 s at which the normal stress becomes negligibly small. The fitting of the relaxation behavior by the relaxation behavior of a single Maxwell element, i.e., a spring with modulus G connected in series to a dashpot with viscosity μ, i.e., relaxation time, $\lambda = \mu/G$, generated $\lambda = 114$ s.

Soltz and Ateshian [29] compressed 0.85 mm thick specimens obtained from the joints of 6-month-old bovine joints, and measured ~0.35 MPa peak reaction stress and ~750 s relaxation time upon 20% compression as compared with 0.42 MPa peak reaction stress observed in our study. In another study using 5% compression at a rate of 0.01 strain/s, DiSilvestro et al. [50] determined ~1.4 MPa peak stress and ~80 s relaxation time (assuming exponential relaxation behavior in conjunction with a single relaxation time on a full thickness mature bovine articular cartilage). Overall, the wide disparities in the relaxation time and peak stress values should reflect the differing natures of the native tissue specimens collected and tested and the nonlinear nature of the experiment.

On the other hand, the relaxation of the tissue constructs cultured over 4 weeks involves significantly shorter relaxation times (Fig. 5). Overall, the time-dependent behaviors of the native tissue and tissue constructs are indicative of the strong role that viscoelasticity plays. In Newtonian fluid behavior the stress imposed on the Newtonian material would decay instantaneously upon the

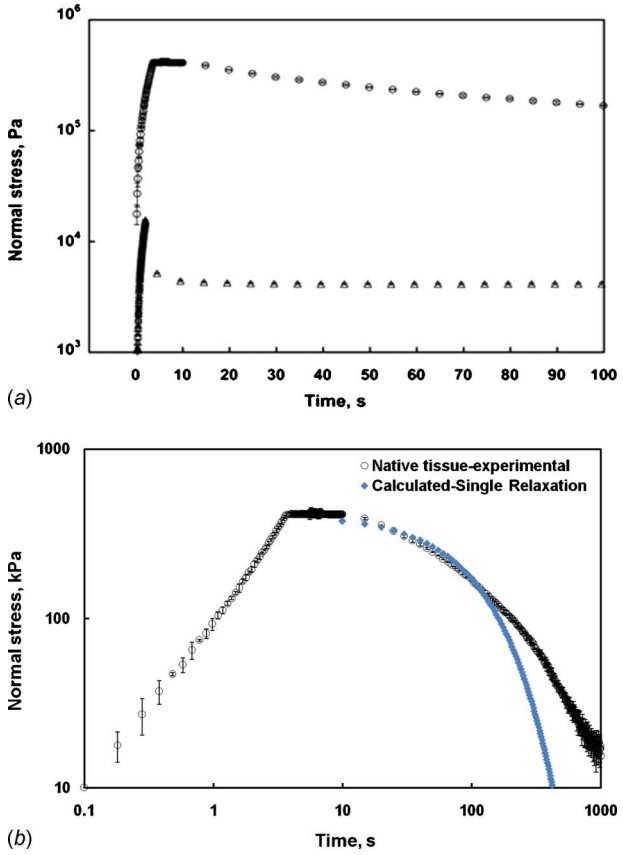

Fig. 5 (*a*) Unconfined compression stress-relaxation response of the native tissue (○) and engineered tissue constructs after four weeks (△) over 100 s. (*b*) Unconfined compression stress-relaxation response of the native tissue over 1000 s and corresponding single relaxation time fit (♦) in the same range. Compression rate is 0.05 mm/s.

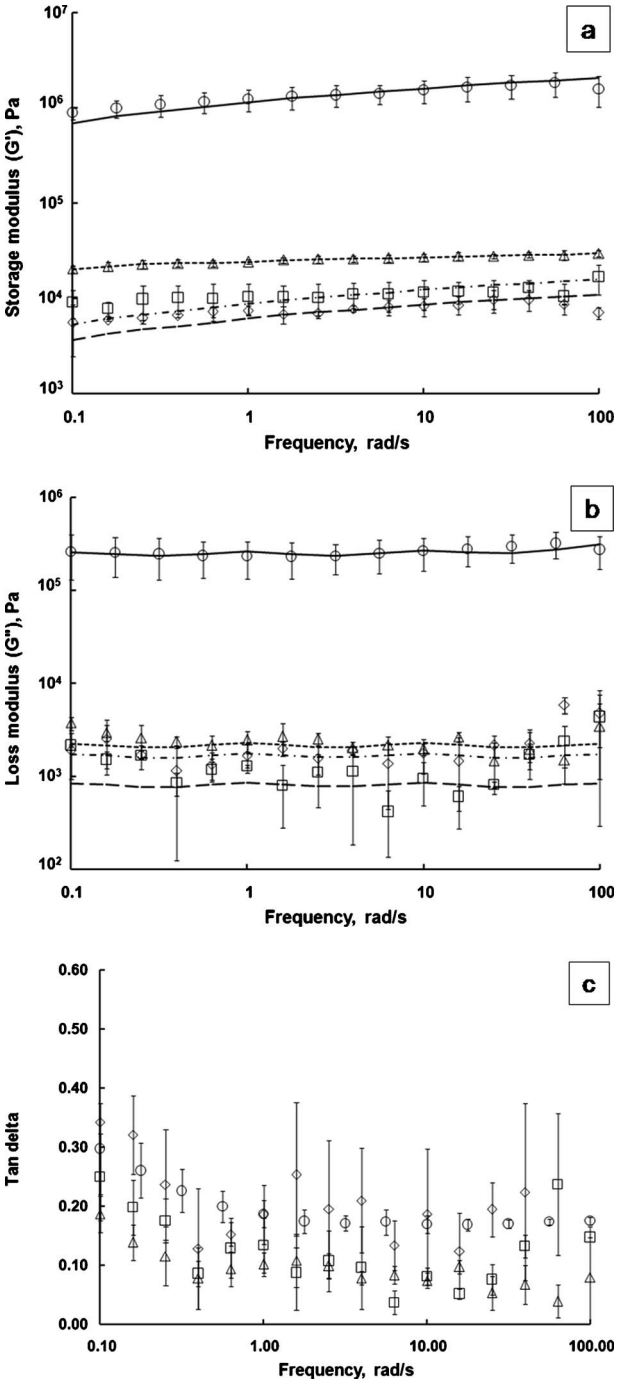

Fig. 6 Frequency dependence of (*a*) the storage modulus, (*b*) the loss modulus, and (*c*) the tan delta of the native tissue (○), tissue constructs after four weeks (△) and one week (□), and the unseeded scaffolds (◇) at 0.1% strain and 37°C. The best fit of the generalized Maxwell model for the native tissue (–), tissue constructs after four weeks (---) and one week (–·–·–), and the unseeded scaffolds (– –) are also provided. Error bars represent the upper and lower bounds of the deviations from the mean for 95% confidence interval (n=3).

cessation of the shearing. On the other hand, for a purely elastic material the stress associated with a strain that is maintained would remain constant. In viscoelastic behavior, however, time-dependent stress relaxation would occur. For polymeric substances, it is the density of the entanglements between the macromolecules, which, in turn, is influenced by the molecular weight distribution of the polymer that controls the relaxation rate. Higher molecular weights lead to greater relaxation times. In tissue constructs the interconnectivity of the cellular structures and the inherent viscoelasticity of the solid matrix constituting the articular cartilage should play important roles to shape the relaxation behavior.

3.2.4 Frequency Dependence of the Linear Viscoelastic Material Functions. The frequency-sweep experiments were performed in the frequency range of 0.1–100 rps at a strain amplitude of 0.1%. At this strain amplitude all four sets of specimens (unseeded scaffold, tissue constructs formed at 1 and 4 weeks and the native tissue) exhibited linear viscoelastic behavior. This frequency range is considered to be physiologically relevant [34], as the cartilage is subjected to cyclic loadings at frequency levels between 1 Hz (~6 rps) during slow walking, which is the predominant motion of the body, and 2.25 Hz (~15 rps) during sprinting [51].

The frequency dependencies of the storage modulus G', loss modulus G'', and tan delta=G''/G' of four sets of samples are shown in Figs. 6(*a*)–6(*c*), respectively. The frequency dependence of the dynamic properties G' and G'' were fitted with the generalized Maxwell model [52,53]

$$G' = \sum_i^N G_i \lambda_i^2 \omega^2 / (1 + (\lambda_i \omega))^2 \quad (1)$$

and

$$G'' = \sum_i^N G_i \lambda_i \omega / (1 + (\lambda_i \omega)^2) \quad (2)$$

where λ_i and G_i are the ith relaxation time and relaxation strength, respectively, ω is the frequency, and N is the total number of relaxation times. Six relaxation times were used, i.e., $N=6$, ranging from 0.001 s to 100 s to generate the acceptable fits of the linear viscoelastic data, as shown in Figs. 6(*a*) and 6(*b*).

The results of the frequency-sweep tests suggest that the viscoelastic behavior of the native tissue, the tissue constructs, and the unseeded scaffolds all exhibit features that are typical of the behavior of a gel. The existence of gel-like behavior is indicated by the frequency independent behavior of the storage modulus (G') and the loss modulus (G'') coupled with the G' and G'' versus the frequency data exhibiting parallel behavior and the much greater values of the storage modulus G' in comparison to those of the loss modulus G'' [54,55]. The storage moduli (G') of the native bovine tissue, the tissue constructs after 4 weeks, the tissue constructs after 1 week, and the unseeded scaffolds were determined to be around 10^6 Pa, 2×10^4 Pa, 9×10^3 Pa, and 7×10^3 Pa, respectively, while their loss moduli (G'') were determined to be around 2×10^5 Pa, 3×10^3 Pa, 2×10^3 Pa, and 2×10^3 Pa, respectively.

Such typical gel-like behavior of native cartilage-bone tissue for which the linear viscoelastic material functions are insensitive to the frequency applied was also observed by Zhu et al. [34] for small compressive strains in the frequency range of 0.01—10 Hz and oscillatory shear deformation. The cartilage portion of the native cartilage-bone interface tissue consists of collagen fibers and proteoglycans in a fluid phase of water and electrolytes [56]. The proteoglycans form molecular networks, which are able to store deformational energy [31,32], while the crosslinked fibrous collagens provide relatively high tensile stiffness and strength [57] to the tissue. The structure of each of the two macromolecules, i.e., collagens and proteoglycans, and their mutual interactions in the matrix together with the hydrodynamics of the interstitial fluid flow thus determine the viscoelastic properties of the interface tissue [33,34]. The availability of the permanent junction points imparted by the crosslinked fibrous collagen molecules allows an affine type deformation upon the application of a stress, therefore furnishing the observed frequency independent gel-like behavior in the native tissue and tissue constructs of our investigation. The phase angle versus the frequency behavior of the native tissue suggests that phase angle decreases from 16.5 to 9.9 in the 0.02–15.9 Hz (0.1–100 rps) range. These values are in the same range of the phase angles noted by Kim et al. [20] and Park et al. [58]. However, the phase angle values of the native tissue remain constant in the 0.3–15.9 Hz (1.8–100 rps) frequency range. This behavior in the 0.3–15.9 Hz (1.8–100 rps) frequency range is different than the phase angle behavior noted by Kim et al. [20] and Park et al. [58], which indicated that the phase angle reduces to zero (purely elastic behavior is attained at the corresponding high Deborah number range) at 1.0 Hz [20] and at 40 Hz [58]. The lack of decrease in the phase angle to zero in our investigation could be associated with the wall slip of the native tissue in the high frequency range of our oscillatory shear experiments, consistent with our observations in the discussion of the strain amplitude dependence of the dynamic data observed in Fig. 4(*b*).

Results of the frequency-sweep experiments also showed that the storage modulus values of the native tissue are significantly higher than those of the engineered tissue constructs and the unseeded scaffolds. Storage modulus values of the engineered tissue constructs after 4 weeks of cell culture are significantly higher than those of the tissue constructs cultured for 1 week. The increase in the elasticity with culture time suggests that the tissue formation progressed with time and that the degree of tissue formation can be evaluated from the values of viscoelastic material functions of the tissue constructs. Overall, the behavior of the tissue constructs is qualitatively similar to that of the native tissue; the values of their material functions are lower than those of the native tissue, but increase with increasing culturing time, suggesting that the linear viscoelastic properties could be used as a precursor of the stage of tissue development.

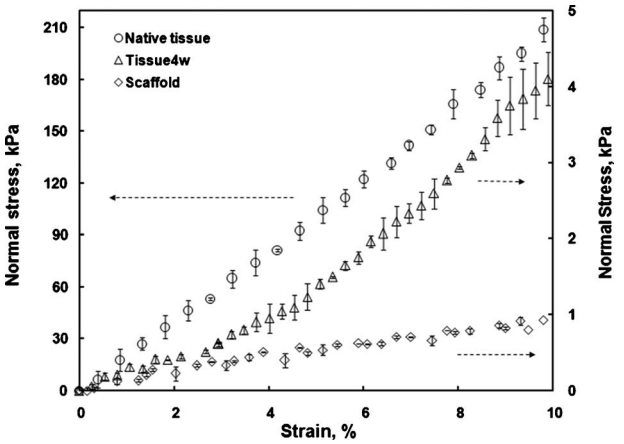

Fig. 7 Stress-strain behavior of native tissue (○), engineered tissue constructs after four weeks (△), and the unseeded scaffolds (◇). Compression rate is 0.05 mm/min. Error bars represent the upper and lower bounds of deviations from the mean for 95% confidence interval.

3.3 Compressive Properties. Biomechanical compression of the specimens was performed under unconfined compression, as there exist analogies between physiological contact loading and unconfined compression. Park et al. [58], for instance, reported several analogies including (i) the uniformity of the interstitial fluid pressurization through the depth and tangential direction of the flow of interstitial fluid to the articular surface at the contact zone, (ii) presence of no compaction boundary layer at the articular surface in the loaded region, and (iii) the stresses generated during physiological movements being tensile in the tangential direction and compressive in the direction normal to the articular surface. The compressive stress-strain behavior of the native bovine cartilage-bone tissue and the tissue constructs obtained upon 4 weeks of culture period are shown in Fig. 7 along with the compressive behavior of the unseeded PCL-β-TCP scaffolds. The normal stresses in compression determined at 10% strain for the unseeded scaffold, the tissue constructs cultured for 4 weeks, and the native tissue were 0.87 ± 0.08 kPa, 3.59 ± 0.34 kPa, and 210.80 ± 8.93 kPa, respectively. The significant differences between the compressive normal stress values obtained for the unseeded scaffolds and tissue constructs cultured for 4 weeks reflect the efficacy of the tissue formation process during the 4 weeks of culturing period. However, it should be noted that the normal stress values of the tissue constructs obtained after 4 weeks of culturing time were approximately two orders of magnitude smaller than those of the native tissue, as shown in Fig. 7.

The Young's modulus (slope of the stress-strain curve in the linear region) and the area under the stress-strain curve of the native tissue, the tissue constructs, as well as the unseeded scaffolds, are presented in Table 1. The Young's modulus values of the native tissue, i.e., 21.315 ± 0.176 kPa, were significantly greater than those of the tissue constructs, i.e., 0.326 ± 0.144 kPa, and the unseeded scaffold samples, i.e., 0.085 ± 0.144 kPa. Under conditions that fracture is achieved during the application of the strain, the integrated area under the stress-strain curve represents the toughness of the specimen where the value of the toughness is related to various mechanical properties including the impact strength of the specimen. In our case since the fracture of the specimen could not be realized within the strain range applied, the reported area under the stress versus strain curve would represent the total mechanical energy per unit volume associated with straining the specimen to the particular strain applied. As ex-

Table 1 Biomechanical properties of the native tissue, engineered tissue constructs, and unseeded PCL-β-TCP scaffolds

	Modulus (kPa)	R^2	Area under stress-strain curve (kPa)
Native tissue	21.315 ± 0.176	99.92 ± 0.054	981.25 ± 0.71
Tissue 4weeks	0.326 ± 0.144	97.69 ± 0.299	12.74 ± 0.58
Unseeded Scaffold	0.085 ± 0.144	97.21 ± 0.306	4.44 ± 0.58

Deviations are standard errors of means and define the lower and upper bounds for the 97.5% confidence interval.
* The difference is significant at p<0.01 level.

pected, the total mechanical energy per unit volume, i.e., the integrated area under the stress-strain curve values of the native tissue, i.e., 981.25 ± 0.71 kPa, were significantly greater than those of the tissue constructs, i.e., 12.74 ± 0.58, and the unseeded scaffold samples, i.e., 4.44 ± 0.58 kPa for the same total strain applied (Fig. 7), emphasizing again that the biomechanical properties of the tissue constructs were inferior as compared with those of the native tissue and considerable development in vivo would be necessary to reach the properties of the native tissue.

In previous studies, the biomechanical properties of bone tissue such as modulus and toughness were used as the predictors for the degree of mineralization, and collagen type-I formation, respectively [59,60]. As shown in Table 1, the modulus of the engineered tissue constructs after 4 weeks of cell culture is significantly higher than that of the unseeded scaffolds, presumably indicating the presence of a high degree of mineralization within 4 weeks. Similarly, the areas under the stress-strain curves of the tissue constructs cultured for 4 weeks are significantly higher than those of the unseeded scaffolds. These findings may suggest the penetration of the cells into the interior of the scaffold and the associated development of the expression of bone related proteins to form the collagenous extracellular matrix throughout the scaffold. As also noted during the comparison of the linear viscoelastic properties of the tissue constructs with those of the native tissue, the time-dependent development of the compressive properties also suggests that the properties of the tissue constructs would continue to evolve with longer incubation times or upon in vivo implementation as the cells continue to proliferate and differentiate.

4 Conclusions

A hybrid twin-screw extrusion-electrospinning process was employed to generate biodegradable scaffolds with linearly distributed β-tricalcium phosphate nanoparticle concentrations to demonstrate the ability to generate gradations in properties that can be subsequently aimed at emulating the gradations found in native-joint tissue. The scaffolds were seeded with pre-osteoblastic MC3T3-E1 cells followed by culturing to generate tissue constructs. The frequency dependent characterization of the linear viscoelastic properties of the tissue constructs indicated that the culturing needs to be carried out for longer durations of time to increase the stiffness of the tissue construct to better approach the strong gel behavior of the native tissue. The time-dependent development of the dynamic properties, especially the increase in the storage modulus values with culturing time, are in line with the findings from the compressive characterization of the tissue constructs, where compressive properties also increase, albeit slowly, toward the values exhibited by native tissue. Characterization of the linear viscoelastic material functions thus furnishes an additional means of assessment of the degree of development of tissue culture constructs.

Acknowledgment

We thank Professor Arthur Ritter and Dr. Halil Gevgilili of Stevens Institute of Technology for their valuable inputs and comments. The consignment of the MPR 7.5 mm twin-screw extruder used for the manufacturing of the biodegradable scaffolds by Material Processing & Research, Inc. and the help received by them during the course of this research are sincerely appreciated. We also thank Dr. Yelda S. Erisken for her help in the statistical analysis of the experimental results.

References

[1] Mankin, H. J., 1982, "The Response of Articular Cartilage to Mechanical Injury," J. Bone Jt. Surg., Am. Vol., **64**(3), pp. 460–466.
[2] Berry, D. J., Harmsen, W. S., Ilstrup, D., Lewallen, D. G., and Cabanela, M. E., 1995, "Survivorship of Uncemented Proximally Porous-Coated Femoral Components," Clin. Orthop. Relat. Res., **319**, pp. 168–177.
[3] Jacobsson, S. A., Djerf, K., and Wahlstrom, O., 1996, "20-Year Results of McKee-Farrar Versus Charnley Prosthesis," Clin. Orthop. Relat. Res., **329**, pp. S60–S68.
[4] Söderman, P., Malchau, H., Herberts, P., Zugner, P., Regner, H., and Garellick, G., 2001, "Outcome After Total Hip Arthroplasty—Part II. Disease-Specific Follow-Up and the Swedish National Total Hip Arthroplasty Register," Acta Orthop. Scand., **72**(2), pp. 113–119.
[5] Kurtz, S., Ong, K., Lau, E., Mowat, F., and Halpern, M., 2007, "Projections of Primary and Revision Hip and Knee Arthroplasty in the United States From 2005 to 2030," J. Bone Jt. Surg., Am. Vol., **89**(4), pp. 780–785.
[6] Mckellop, H. A., Campbell, P., Park, S. H., Schmalzried, T. P., Grigoris, P., Amstutz, H. C., and Sarmiento, A., 1995, "The Origin of Submicron Polyethylene Wear Debris in Total Hip-Arthroplasty," Clin. Orthop. Relat. Res., **311**, pp. 3–20.
[7] Urban, R. M., Tomlinson, M. J., Hall, D. J., and Jacobs, J. J., 2004, "Accumulation in Liver and Spleen of Metal Particles Generated at Nonbearing Surfaces in Hip Arthroplasty," J. Arthroplasty, **19**(8), pp. 94–101.
[8] Jiranek, W. A., Hanssen, A. D., and Greenwald, A. S., 2006, "Antibiotic-Loaded Bone Cement for Infection Prophylaxis in Total Joint Replacement," J. Bone Jt. Surg., Am. Vol., **88**(11), pp. 2487–2500.
[9] Redman, S. N., Oldfield, S. F., and Archer, C. W., 2005, "Current Strategies for Articular Cartilage Repair," Eur. Cells Mater, **9**, pp. 23–32.
[10] Kinner, B., Capito, R. M., and Spector, M., 2005, "Regeneration of Articular Cartilage," *Regenerative Medicine II: Clinical and Preclinical Applications*, I. V. Yannas, ed., Springer-Verlag, Berlin Heidelberg, Vol. 94, pp. 91–123.
[11] Mikos, A. G., Herring, S. W., Ochareon, P., Elisseeff, J., Lu, H. H., Kandel, R., Schoen, F. J., Toner, M., Mooney, D., Atala, A., Dyke, M. E., Kaplan, D., and Vunjak-Novakovic, G., 2006, "Engineering Complex Tissues," Tissue Eng., **12**(12), pp. 3307–3339.
[12] Gomez, S., Toffanin, R., Bernstorff, S., Romanello, M., Amenitsch, H., Rappolt, M., Rizzo, R., and Vittur, F., 2000, "Collagen Fibrils Are Differently Organized in Weight-Bearing and Not-Weight-Bearing Regions of Pig Articular Cartilage," J. Exp. Zool., **287**(5), pp. 346–352.
[13] An, Y. H., and Martin, K. L., 2003, *Handbook of Histology Methods for Bone and Cartilage*, Humana, Clifton, NJ.
[14] Zizak, I., Roschger, P., Paris, O., Misof, B. M., Berzlanovich, A., Bernstorff, S., Amenitsch, H., Klaushofer, K., and Fratzl, P., 2003, "Characteristics of Mineral Particles in the Human Bone/Cartilage Interface," J. Struct. Biol., **141**(3), pp. 208–217.
[15] Bradley, D. A., Muthuvelu, P., Ellis, R. E., Green, E. M., Attenburrow, D., Barrett, R., Arkill, K., Colridge, D. B., and Winlove, C. P., 2007, "Characterisation of Mineralisation of Bone and Cartilage: X-Ray Diffraction and Ca and SrK Alpha X-Ray Fluorescence Microscopy," Nucl. Instrum. Methods Phys. Res. B, **263**(1), pp. 1–6.
[16] Sharma, B., and Elisseeff, J. H., 2004, "Engineering Structurally Organized Cartilage and Bone Tissues," Ann. Biomed. Eng., **32**(1), pp. 148–159.
[17] Mow, V. C., Holmes, M. H., and Lai, W. M., 1984, "Fluid Transport and Mechanical-Properties of Articular-Cartilage—A Review," J. Biomech., **17**(5), pp. 377–394.
[18] Boschetti, F., Pennati, G., Gervaso, F., Peretti, G. M., and Dubini, G., 2004, "Biomechanical Properties of Human Articular Cartilage Under Compressive Loads," Biorheology, **41**(3–4), pp. 159–166.
[19] Oloyede, A., and Broom, N. D., 1991, "Is Classical Consolidation Theory Applicable to Articular-Cartilage Deformation?," Clin. Biomech. (Bristol,

Avon), **6**(4), pp. 206–212.
[20] Kim, Y. J., Bonassar, L. J., and Grodzinsky, A. J., 1995, "The Role of Cartilage Streaming Potential, Fluid Flow and Pressure in the Stimulation of Chondrocyte Biosynthesis During Dynamic Compression," J. Biomech., **28**(9), pp. 1055–1066.
[21] Verteramo, A., and Seedhom, B. B., 2004, "Zonal and Directional Variations in Tensile Properties of Bovine Articular Cartilage With Special Reference to Strain Rate Variation," Biorheology, **41**(3–4), pp. 203–213.
[22] Elliott, D. M., Narmoneva, D. A., and Setton, L. A., 2002, "Direct Measurement of the Poisson's Ratio of Human Patella Cartilage in Tension," ASME J. Biomech. Eng., **124**(2), pp. 223–228.
[23] Hayes, W. C., and Mockros, L. F., 1971, "Viscoelastic Properties of Human Articular Cartilage," J. Appl. Physiol., **31**(4), pp. 562–568.
[24] Magnussen, R. A., Guilak, F., and Vail, T. P., 2005, "Cartilage Degeneration in Post-Collapse Cases of Osteonecrosis of the Human Femoral Head: Altered Mechanical Properties in Tension, Compression, and Shear," J. Orthop. Res., **23**(3), pp. 576–583.
[25] Schinagl, R. M., Gurskis, D., Chen, A. C., and Sah, R. L., 1997, "Depth-Dependent Confined Compression Modulus of Full-Thickness Bovine Articular Cartilage," J. Orthop. Res., **15**(4), pp. 499–506.
[26] Klein, T. J., Chaudhry, M., Bae, W. C., and Sah, R. L., 2007, "Depth-Dependent Biomechanical and Biochemical Properties of Fetal, Newborn, and Tissue-Engineered Articular Cartilage," J. Biomech., **40**(1), pp. 182–190.
[27] Taylor, S. J. G., Walker, P. S., Perry, J. S., Cannon, S. R., and Woledge, R., 1998, "The Forces in the Distal Femur and the Knee During Walking and Other Activities Measured by Telemetry," J. Arthroplasty, **13**(4), pp. 428–437.
[28] Parsons, J. R., and Black, J., 1977, "Viscoelastic Shear Behavior of Normal Rabbit Articular-Cartilage," J. Biomech., **10**(1), pp. 21–29.
[29] Soltz, M. A., and Ateshian, G. A., 2000, "A Conewise Linear Elasticity Mixture Model for the Analysis of Tension-Compression Nonlinearity in Articular Cartilage," ASME J. Biomech. Eng., **122**(6), pp. 576–586.
[30] Huang, C. Y., Mow, V. C., and Ateshian, G. A., 2001, "The Role of Flow-Independent Viscoelasticity in the Biphasic Tensile and Compressive Responses of Articular Cartilage," ASME J. Biomech. Eng., **123**(5), pp. 410–417.
[31] Li, L. P., and Herzog, W., 2004, "The Role of Viscoelasticity of Collagen Fibers in Articular Cartilage: Theory and Numerical Formulation," Biorheology, **41**(3–4), pp. 181–194.
[32] Hayes, W. C., and Bodine, A. J., 1978, "Flow-Independent Viscoelastic Properties of Articular-Cartilage Matrix," J. Biomech., **11**(8–9), pp. 407–419.
[33] Spirt, A. A., Mak, A. F., and Wassell, R. P., 1989, "Nonlinear Viscoelastic Properties of Articular-Cartilage in Shear," J. Orthop. Res., **7**(1), pp. 43–49.
[34] Zhu, W., Mow, V. C., Koob, T. J., and Eyre, D. R., 1993, "Viscoelastic Shear Properties of Articular Cartilage and the Effects of Glycosidase Treatments," J. Orthop. Res., **11**(6), pp. 771–781.
[35] Schaefer, D., Martin, I., Shastri, P., Padera, R. F., Langer, R., Freed, L. E., and Vunjak-Novakovic, G., 2000, "In Vitro Generation of Osteochondral Composites," Biomaterials, **21**(24), pp. 2599–2606.
[36] Gao, J., Dennis, J. E., Solchaga, L. A., Awadallah, A. S., Goldberg, V. M., and Caplan, A. I., 2001, "Tissue-Engineered Fabrication of an Osteochondral Composite Graft Using Rat Bone Marrow-Derived Mesenchymal Stem Cells," Tissue Eng., **7**(4), pp. 363–371.
[37] Sherwood, J. K., Riley, S. L., Palazzolo, R., Brown, S. C., Monkhouse, D. C., Coates, M., Griffith, L. G., Landeen, L. K., and Ratcliffe, A., 2002, "A Three-Dimensional Osteochondral Composite Scaffold for Articular Cartilage Repair," Biomaterials, **23**(24), pp. 4739–4751.
[38] Hung, C. T., Lima, E. G., Mauck, R. L., Taki, E., LeRoux, M. A., Lu, H. H., Stark, R. G., Guo, X. E., and Ateshian, G. A., 2003, "Anatomically Shaped Osteochondral Constructs for Articular Cartilage Repair," J. Biomech., **36**(12), pp. 1853–1864.
[39] Davisson, T., Kunig, S., Chen, A., Sah, R., and Ratcliffe, A., 2002, "Static and Dynamic Compression Modulate Matrix Metabolism in Tissue Engineered Cartilage," J. Orthop. Res., **20**(4), pp. 842–848.
[40] Angele, P., Yoo, J. U., Smith, C., Mansour, J., Jepsen, K. J., Nerlich, M., and Johnstone, B., 2003, "Cyclic Hydrostatic Pressure Enhances the Chondrogenic Phenotype of Human Mesenchymal Progenitor Cells Differentiated In Vitro," J. Orthop. Res., **21**(3), pp. 451–457.
[41] Erisken, C., Kalyon, D. M., and Wang, H., 2008, "Functionally Graded Electrospun Polycaprolactone and Beta-Tricalcium Phosphate Nanocomposites for Tissue Engineering Applications," Biomaterials, **29**(30), pp. 4065–4073.
[42] Erisken, C., Kalyon, D. M., and Wang, H. J., 2008, "A Hybrid Twin Screw Extrusion/Electrospinning Method to Process Nanoparticle-Incorporated Electrospun Nanofibres," Nanotechnology, **19**(16), 165302 (8 pp).
[43] Armstrong, C. G., Bahrani, A. S., and Gardner, D. L., 1979, "In Vitro Measurement of Articular Cartilage Deformations in the Intact Human Hip Joint Under Load," J. Bone Jt. Surg., Am. Vol., **61**(5), pp. 744–755.
[44] Macirowski, T., Tepic, S., and Mann, R. W., 1994, "Cartilage Stresses in the Human Hip-Joint," ASME J. Biomech. Eng., **116**(1), pp. 10–18.
[45] Eckstein, F., Lemberger, B., Stammberger, T., Englmeier, K. H., and Reiser, M., 2000, "Patellar Cartilage Deformation In Vivo After Static Versus Dynamic Loading," J. Biomech., **33**(7), pp. 819–825.
[46] Kalyon, D. M., Yaras, P., Aral, B., and Yilmazer, U., 1993, "Rheological Behavior of a Concentrated Suspension—A Solid Rocket Fuel Simulant," J. Rheol., **37**(1), pp. 35–53.
[47] Aral, B. K., and Kalyon, D. M., 1994, "Effects of Temperature and Surface-Roughness on Time-Dependent Development of Wall Slip in Steady Torsional Flow of Concentrated Suspensions," J. Rheol., **38**(4), pp. 957–972.
[48] Jay, G. D., Tantravahi, U., Britt, D. E., Barrach, H. J., and Cha, C. J., 2001, "Homology of Lubricin and Superficial Zone Protein (SZP): Products of Megakaryocyte Stimulating Factor (MSF) Gene Expression by Human Synovial Fibroblasts and Articular Chondrocytes Localized to Chromosome 1q25," J. Orthop. Res., **19**(4), pp. 677–687.
[49] Kalyon, D. M., 2005, "Apparent Slip and Viscoplasticity of Concentrated Suspensions," J. Rheol., **49**(3), pp. 621–640.
[50] DiSilvestro, M. R., Zhu, Q. L., and Suh, J. K. F., 2001, "Biphasic Poroviscoelastic Simulation of the Unconfined Compression of Articular Cartilage: II—Effect of Variable Strain Rates," ASME J. Biomech. Eng., **123**(2), pp. 198–200.
[51] Barker, M. K., and Seedhom, B. B., 2001, "The Relationship of the Compressive Modulus of Articular Cartilage With Its Deformation Response to Cyclic Loading: Does Cartilage Optimize Its Modulus so as to Minimize the Strains Arising in it Due to the Prevalent Loading Regime?," Rheumatology (Oxford), **40**(3), pp. 274–284.
[52] Bird, R. B., Armstrong, R. C., and Hassager, O., 1987, *Dynamics of Polymeric Liquids: Fluid Mechanics*, 2nd ed., Wiley, New York.
[53] Kalyon, D. M., Yu, D., and Yu, J., 1988, "Melt Rheology of Two Engineering Plastics: Poly(Ether Imide) and Poly (2,6-Dimethyl-1,4 Phenylene Ether)," J. Rheol., **32**(8), pp. 789–811.
[54] Chambon, F., and Winter, H. H., 1987, "Linear Viscoelasticity at the Gel Point of A Cross-Linking PDMS With Imbalanced Stoichiometry," J. Rheol., **31**(8), pp. 683–697.
[55] De Rosa, M. E., and Winter, H. H., 1994, "The Effect of Entanglements on the Rheological Behavior of Polybutadiene Critical Gels," Rheol. Acta, **33**(3), pp. 220–237.
[56] Stading, M., and Langer, R., 1999, "Mechanical Shear Properties of Cell-Polymer Cartilage Constructs," Tissue Eng., **5**(3), pp. 241–250.
[57] Akizuki, S., Mow, V. C., Muller, F., Pita, J. C., Howell, D. S., and Manicourt, D. H., 1986, "Tensile Properties of Human Knee Joint Cartilage: I. Influence of Ionic Conditions, Weight Bearing, and Fibrillation on the Tensile Modulus," J. Orthop. Res., **4**(4), pp. 379–392.
[58] Park, S., Hung, C. T., and Ateshian, G. A., 2004, "Mechanical Response of Bovine Articular Cartilage Under Dynamic Unconfined Compression Loading at Physiological Stress Levels," Osteoarthritis Cartilage, **12**(1), pp. 65–73.
[59] Garnero, P., Borel, O., Gineyts, E., Duboeuf, F., Solberg, H., Bouxsein, M. L., Christiansen, C., and Delmas, P. D., 2006, "Extracellular Post-Translational Modifications of Collagen Are Major Determinants of Biomechanical Properties of Fetal Bovine Cortical Bone," Bone, **38**(3), pp. 300–309.
[60] Burr, D. B., 2002, "The Contribution of the Organic Matrix to Bone's Material Properties," Bone, **31**(1), pp. 8–11.